Non-Lifshitz-Kosevich field-and temperature-dependent amplitude of quantum oscillations in the quasi-two dimensional metal θ-(ET) 4 ZnBr 4 (C 6 H 4 Cl 2)

Alain Audouard, Jean-Yves Fortin, David Vignolles, Rustem I Lyubovskii, Loïc Drigo, Gena V. Shilov, Fabienne Duc, Elena I Zhilyaeva, Rimma N Lyubovskaya, Enric Canadell

PAPER

Non-Lifshitz–Kosevich field- and temperature-dependent amplitude of quantum oscillations in the quasi-two dimensional metal θ-$(ET)_4ZnBr_4(C_6H_4Cl_2)$

IOP Publishing Journal of Physics: Condensed Matter
J. Phys.: Condens. Matter **27** (2015) 315601 (7pp) doi:10.1088/0953-8984/27/31/315601

Non-Lifshitz–Kosevich field- and temperature-dependent amplitude of quantum oscillations in the quasi-two dimensional metal θ-$(ET)_4ZnBr_4(C_6H_4Cl_2)$

Alain Audouard[1], Jean-Yves Fortin[2], David Vignolles[1], Rustem B Lyubovskii[3], Loïc Drigo[1], Gena V Shilov[3], Fabienne Duc[1], Elena I Zhilyaeva[3], Rimma N Lyubovskaya[3] and Enric Canadell[4]

[1] Laboratoire National des Champs Magnétiques Intenses (UPR 3228 CNRS, INSA, UJF, UPS) 143 avenue de Rangueil, F-31400 Toulouse, France
[2] Institut Jean Lamour, Département de Physique de la Matière et des Matériaux, CNRS-UMR 7198, Vandoeuvre-les-Nancy, F-54506, France
[3] Institute of Problems of Chemical Physics, Russian Academy of Sciences, 142432 Chernogolovka, MD, Russia
[4] Institut de Ciència de Materials de Barcelona, CSIC, Campus de la UAB, 08193, Bellaterra, Spain

E-mail: alain.audouard@lncmi.cnrs.fr

Received 11 May 2015, revised 16 June 2015
Accepted for publication 22 June 2015
Published 20 July 2015

Abstract

According to band structure calculations, the Fermi surface of the quasi-two dimensional metal θ-$(ET)_4ZnBr_4(C_6H_4Cl_2)$ illustrates the linear chain of coupled orbits model. Accordingly, de Haas–van Alphen oscillations spectra recorded in pulsed magnetic field of up to 55 T evidence many Fourier components, the frequency of which are linear combinations of the frequencies relevant to the closed α and the magnetic breakdown β orbits. The field and temperature dependence of their amplitude are quantitatively accounted for by analytic calculations including, beyond the Lifshitz–Kosevich formula, second-order terms in damping factors due to the oscillation of the chemical potential as the magnetic field varies. Whereas these second-order terms are negligible for the orbits α, β and $2\beta - \alpha$, they are solely responsible for the 'forbidden orbit' $\beta - \alpha$ and its harmonic and have a significant influence on Fourier components such as 2α and $\beta + \alpha$, yielding strongly non-Lifshitz–Kosevich behaviour in the latter case.

Keywords: de Haas–van Alphen oscillations, organic metals, high magnetic fields

(Some figures may appear in colour only in the online journal)

1. Introduction

Many quasi-two-dimensional (q-2D) metals, in particular charge transfer salts based on the bis-ethylenedithio-tetrathiafulvalene (ET) molecule, illustrate the textbook Fermi surface (FS) proposed by Pippard in the early sixties. This model FS, an example of which is provided in the inset of figure 1, was intended to compute the de Haas–van Alphen (dHvA) oscillation spectrum of the linear chain of orbits coupled by magnetic breakdown (MB) [1, 2]. In line with the coupled orbits network model of Falicov–Stachowiak [2, 3], relevant dHvA oscillations spectra involve linear combinations of frequencies linked to the α and MB-induced β orbits [4–9]. However, it is now well established that the field and temperature dependence of many of these Fourier components cannot be accounted for by this model due to oscillation of the chemical potential in magnetic field [10–16]. Analytic tools, given in the Appendix, have been provided in order to quantitatively

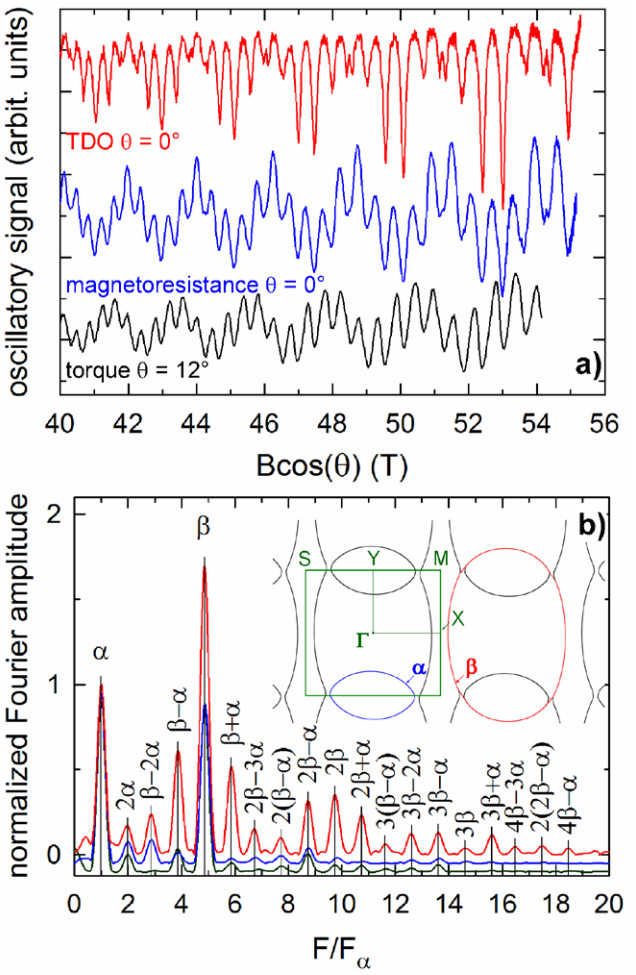

Figure 1. (a) Oscillatory part of the high field range of TDO frequency (crystal #6), 4-point interlayer magnetoresistance (crystal #5) and torque (crystal #1) data at 2 K and (b) corresponding Fourier analysis (Fourier spectra are shifted down from each other by a constant amount for clarity). Thin lines in (b) are marks calculated with $F_\alpha = 0.93$ kT and $F_\alpha/F_\beta = 0.205$. The inset displays the Fermi surface of the conducting layer at 100 K. Green rectangle depicts the first Brillouin zone where $S = (-a^*/2, b^*/2)$, $Y = (0, b^*/2)$, $M = (a^*/2, b^*/2)$, $X = (a^*/2, 0)$ and $\Gamma = (0, 0)$. The basic orbits α and β are marked by the blue and red lines, respectively.

account for the field- and temperature-dependent amplitudes of the various Fourier components observed [17–19]. Briefly, in addition to a first-order term corresponding to the Lifshitz–Kosevich (LK) model [2], second-order terms due to oscillation of the chemical potential must be taken into account. Nevertheless, their relative importance strongly depends on the involved parameter values, in particular the Landé factors. As an example, provided spin damping factors relevant to basic orbits are not too small, i. e. $g^*_\alpha m_\alpha$ and $g^*_\beta m_\beta$ (where $g^*_{\alpha(\beta)}$ and $m_{\alpha(\beta)}$ are the effective Landé factor and effective mass, respectively, of the $\alpha(\beta)$ orbit) are not close to odd integers, these second-order terms have a negligible contribution to the Fourier amplitude A_α and A_β, respectively. In contrast, the amplitudes $A_{p(\beta-\alpha)}$ of the Fourier components with frequencies $p(F_\beta - F_\alpha)$, which are commonly referred to as 'forbidden orbits' since they do not correspond to MB orbits, are only governed by second-order terms. For completeness, It should be noticed that, in the case of magnetoresistance oscillations, components such as $\beta - \alpha$ or $\beta - 2\alpha$ correspond to quantum interference paths [20] which are liable to enter the Shubnikov–de Haas (SdH) spectra [21].

Up to now, these calculations have only been implemented to account for the data of the strongly two-dimensional compound θ-$(ET)_4CoBr_4(C_6H_4Cl_2)$ [17, 18], referred in the following to as the Co-compound. For this compound, the field and temperature dependence of the second harmonic amplitude of the α orbit ($A_{2\alpha}$), which significantly differs from the predictions of the LK model, and the 'forbidden orbit' amplitude $A_{\beta-\alpha}$ are quantitatively accounted for by the calculations. Nevertheless, data analysis for other compounds, with different FS parameters, are needed to further check the model. In addition, depending on the value of the involved FS parameters (in particular effective masses and Landé factors), strongly non-monotonic field and temperature dependence is liable to be observed in few cases [17, 19]. Actually, such a feature has never been reported yet.

The aim of this article is to report on quantum oscillations spectra of θ-$(ET)_4ZnBr_4(C_6H_4Cl_2)$, referred to as the Zn-compound in the following. This compound belongs to the same family as the Co-compound, namely θ-$(ET)_4MBr_4(C_6H_4Cl_2)$, where M is a metal such as Co, Zn, Hg, Cd (for a review, see [22]). Strikingly, the crystal structure of these compounds involves one conducting and one insulating ET plane, with different atomic arrangement, insuring a strong two-dimensionality. More extended data than for the previously reported Co-compound, i.e. field and temperature dependence of Fourier amplitude relevant to several frequency combinations, are derived, allowing a more extensive check of the formulas reported in the Appendix. In particular, it is demonstrated that strongly non-monotonic temperature dependence of the Fourier component with frequency corresponding to the MB orbit $\beta+\alpha$ is observed.

2. Experimental

Crystals were synthesized by electrocrystallization technique as reported in [23]. The FS topology was obtained through extended Hückel type tight-binding band structure calculations [24], as reported in [25, 26]. These calculations were based on x-ray diffraction data collected at 100 K and 180 K at the IPCP-Chernogolovka and the LCC-Toulouse, respectively.

Six crystals denoted hereafter as crystal #1 to #6, respectively, were studied in pulsed magnetic fields of up to 55 T with a pulse decay duration of 0.32 s. DHvA oscillations were measured through magnetic torque measurements of crystals #1 to #4, with approximate dimensions $0.1 \times 0.1 \times 0.04$ mm^3, stuck on a microcantilever. Variations of the microcantilever piezoresistance were measured at liquid helium temperatures with a Wheatstone bridge with an *ac* excitation at a frequency of 63 kHz. The angle between the normal to the conducting plane and the magnetic field direction was $\theta = 12°, 8°$ and $9°$ for crystals #1, #2 and #3, respectively, while θ was varied from 15° to 71° thanks to a rotating sample holder for crystal #4. SdH oscillations were measured through 4-point interlayer

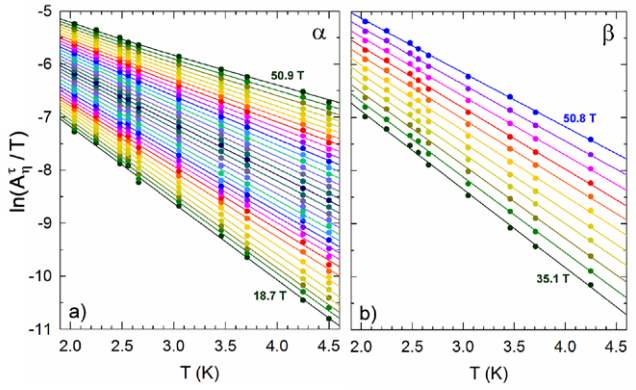

Figure 2. Temperature dependence (mass plots) of the magnetic torque amplitudes (a) A_α^τ and (b) A_β^τ. Solid lines in (a) and (b) are best fits of equations (A.1) and (A.3), respectively, to the data. They are obtained with $m_\alpha = 1.85, m_\beta = 3.4, B_0 = 26$ T and $T_D = 0.8$ K. The considered magnetic field values are evenly spaced in 1/B in the explored field range, the boundary of which are indicated in the figures.

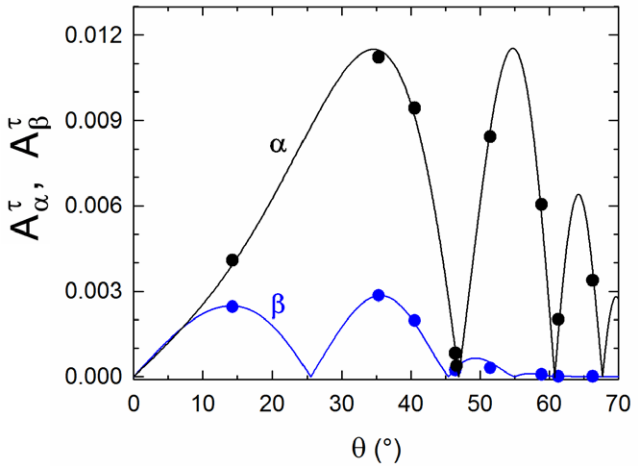

Figure 3. Angle dependence of the magnetic torque amplitudes A_α^τ and A_β^τ. Solid lines are best fits of equations (A.1) and (A.3) to the data for A_α^τ and A_β^τ, respectively. They are obtained with the same effective mass and MB field as in figure 2 and $g_\alpha^* = g_\beta^* = 1.85$.

magnetoresistance (crystal #5) and contactless tunnel diode oscillator (TDO)-based method [17, 27] (crystal #6).

3. Results and discussion

In the next section 3.1 the oscillatory data are examined at the light of band structure calculations. Section 3.2 reports on the field and temperature dependence of the basic Fourier components, linked to the α and β orbits, observed in dHvA and SdH spectra while dHvA frequency combinations are considered in section 3.3.

3.1. Band structure calculations and oscillatory spectrum

Crystalline and electronic band structures of the Zn-compound are very similar to those of the Co-compound. Briefly, two different cation layers, labeled *A* and *B*, respectively, in [17, 22, 23], with different atomic arrangements, are observed within the unit cell. According to band structure calculations, layer *A* with α-type packing is insulating while layer *B* with θ-type packing is conducting (for details regarding atomic packing in organic metals, see [28]). As reported in figure 1, the FS topology relevant to layer *B* illustrates the Pippard's model, observed in many organic conductors based on the ET molecule. Namely, it is composed of one q-2D closed tube and two q-1D sheets separated by a gap. In magnetic fields, the closed tube yields the α orbit while, thanks to MB, the β orbit with an area equal to that of the first Brillouin zone (FBZ) is observed. The area of the α orbit is 17.0% and 18.2% of the FBZ area at 180 K and 100 K, respectively. It can be remarked that the FS of figure 1 differs from that of other θ-phase salts. In these latter salts the anions impose a periodicity along the *b* direction which is different from that observed in the Zn- and Co-compounds, yielding different FS topology [29].

Figure 1(a) displays oscillatory parts of the magnetic torque, 4-point longitudinal magnetoresistance and TDO data

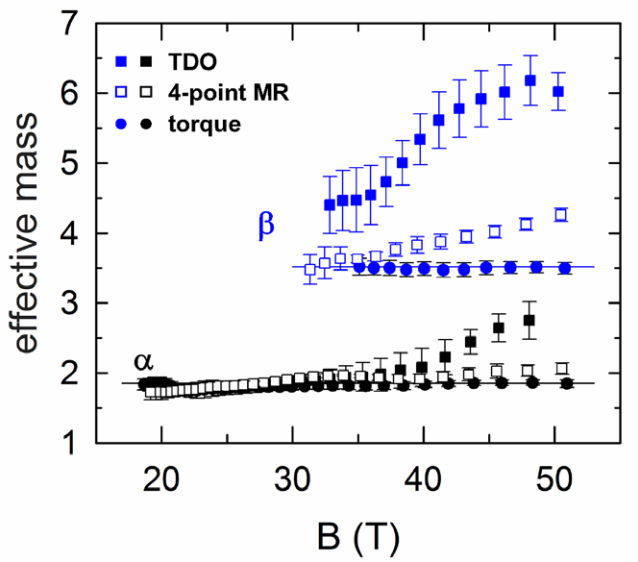

Figure 4. Field dependence of the effective mass value of α and β orbits derived from magnetic torque, 4-point magnetoresistance and TDO data. Horizontal lines mark the effective mass values deduced from magnetic torque data, yielding dHvA oscillations, $m_\alpha = 1.85$ and $m_\beta = 3.4$.

at 2 K. It can be remarked first that, while TDO and 4-point magnetoresistance data are in phase, magnetic torque data are phase-shifted by $\pi/2$. This feature indicates that, while magnetic torque yields dHvA oscillations, both TDO and 4-point magnetoresistance yield SdH oscillations, in agreement with previous statements [30, 31]. Corresponding Fourier analysis are displayed in figure 1(b). The two main frequencies, $F_\alpha = 0.930(2)$ kT and $F_\beta = 4.534(7)$ kT, correspond to the α and β orbits, respectively, hence the α orbit area amounts to 20.5% of the FBZ area. This value is in good agreement with the above reported band structure calculations which are based on x-ray diffraction data measured at higher temperature, owing to the increase of the closed tube area relatively

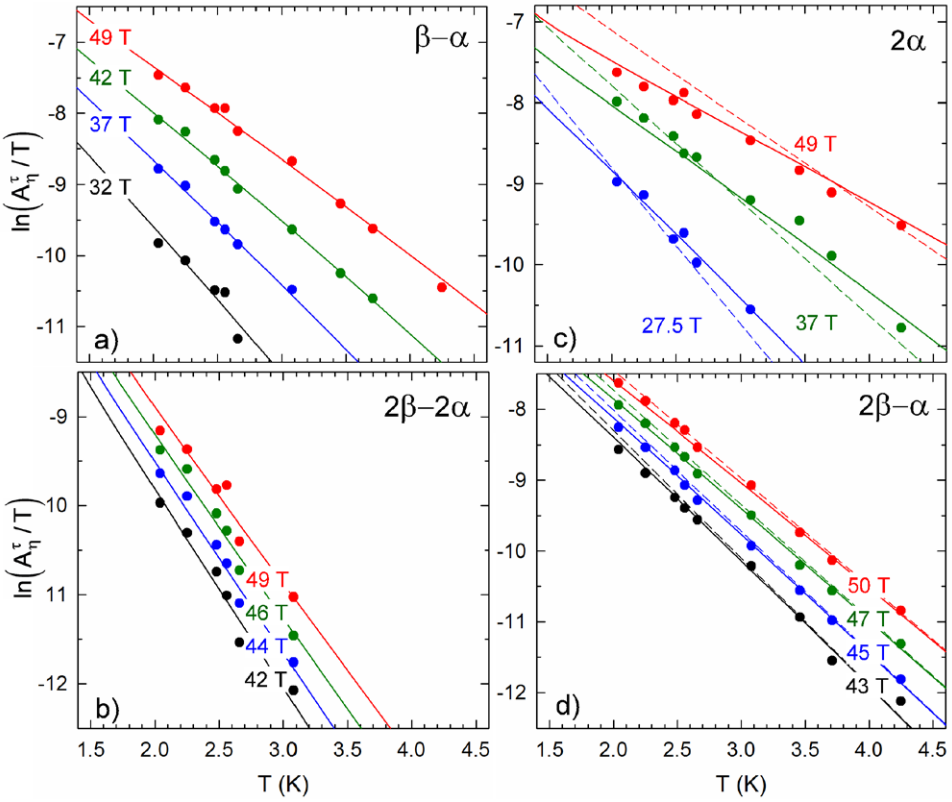

Figure 5. Mass plot of magnetic torque amplitudes for different values of the magnetic field of (a) $\beta - \alpha$, (b) $2(\beta - \alpha)$, (c) 2α and (d) $2\beta - \alpha$. Solid lines in (a)–(d) are calculated with equations (A.2), (A.5), (A.6) and (A.8), respectively. They are obtained with the same set of parameters as in figures 2 and 3. Dashed lines in (c) and (d) are obtained with the Lifshitz–Kosevich formula.

to that of the FBZ, as the temperature decreases from 180 K to 100 K. Strikingly, an unprecedented number of frequencies is observed, in particular in the case of the TDO data, accounting for the strong non-sinusoidal oscillatory part of these data. These frequencies, labeled F_η in the following, are linear combinations of F_α and F_β. Frequency as high as 17.2 kT, corresponding to $\eta = 4\beta - \alpha$, is observed in the TDO spectrum of figure 1.

3.2. Basic Fourier components amplitude

Let us consider first magnetic torque data, the oscillation spectra of which involve Fourier components with frequencies F_η and amplitudes A_η^τ. Since we are dealing with a 2D metal, these amplitudes are related to dHvA oscillations amplitudes A_η as $A_\eta \propto A_\eta^\tau/B \tan(\theta)$ where θ is the angle between the magnetic field direction and the normal to the conducting plane. According to the LK formula, $\ln(A_\eta^\tau/T)$ is predicted to vary linearly with the temperature at a given magnetic field value (mass plot) at high T/B ratio. Since crystals #1, #2 and #3 yield same results within the error bars reported below, we focus in the following on the data relevant to crystal #3, with the lowest Dingle temperature. Data for $\eta = \alpha$ and β are reported in figure 2. They can be analyzed through equations (A.1) and (A.3), respectively. However, no fewer than seven parameters enter these equations: effective masses $m_{\alpha(\beta)}$, Dingle temperatures $T_{D\alpha(\beta)}$, effective Landé factors $g^*_{\alpha(\beta)}$ and MB field B_0. Nevertheless, as observed in the case of the Co-compound [17] and discussed in [18], the second-order terms of equations (A.1) and (A.3) are negligibly small compared to their leading terms, provided the spin damping factors $R^s_{\alpha(\beta)}$ are far enough from spin-zeroes. As a result, the LK model applies and the spin damping factors act as field- and temperature-independent prefactors. However, in addition to the effective masses, the MB field B_0 and the Dingle temperatures $T_{D\alpha(\beta)}$ govern the field dependence of $A_{\alpha(\beta)}$. As a result, each of the two equations (A.1) and (A.3) still involve 3 parameters yielding large uncertainties. For this reason, it is assumed in the following that $T_{D\alpha} = T_{D\beta}$. Within this assumption, data yield $m_\alpha = 1.85(10), m_\beta = 3.40(15)$ and $B_0 = 26(3)$ T for all the three studied crystals. The Dingle temperature, which is the only crystal-dependent parameter is $T_{D1} = 0.9(1)$ K, $T_{D2} = 1.1(1)$ K and $T_{D3} = 0.8(1)$ K for crystal #1–#3, respectively. Effective Landé factors $g^*_{\alpha(\beta)}$, which are the remaining parameters to be determined, are obtained through the angle dependence of $A_{\alpha(\beta)}$. Solid lines in figure 3 are the best fits of equations (A.1) and (A.3) to the data relevant to crystal #4, yielding $g^*_\alpha = g^*_\beta = 1.85(10)$.

In short, the effective masses and Dingle temperatures of the Zn-compound are close to the data obtained for the Co-compound whereas the MB field of the latter is higher [17]. Owing to the effective Landé factors values, which were only estimated in [17], the second-order terms of equations (A.1) and (A.3) are negligible in the field and temperature range

explored, indicating that the LK model, i.e. the first-order term of equations (A.1) and (A.3) satisfactorily accounts for the basic orbits α and β, respectively.

A hallmark of the validity of the LK formula is the field-independency of the effective mass derived through this formula from the temperature dependence of the amplitude, as it can be observed in figure 4 for the dHvA data. In contrast, an apparent strong increase of the effective mass is observed in the case of TDO and, to a less extent, of the 4-point interlayer magnetoresistance data. This behaviour can be ascribed to the failure of the LK formula for SdH oscillations relevant to basic orbits of q-2D metals [32–34]. This feature, which is beyond the scope of the present study focused on dHvA spectra, requires specific calculations of the conductivity [35–38] taking into account the multiband nature of the FS. As for the smaller discrepancy observed for 4-point magnetoresistance compared to contactless TDO measurements, it must be considered that interlayer resistance (R_{zz}) and in-plane resistance (R_{xx}) which are governed by different matrix elements [38], are measured in the former and latter case, respectively. Besides, the electrical contacts on the crystal, in the case of 4-point magnetoresistance, connect the quasi-particles to a non-quantized reservoir, liable to induce a damping of the chemical potential oscillation [34].

3.3. Frequency combinations

Since the parameters entering equations (A.1)–(A.8) are determined from the analysis of the data relevant to the α and β orbits, the field and temperature dependence of all the other Fourier components amplitude should be accounted for by these parameters. As examples, the behaviour of few of these amplitudes is considered in figure 5: a very good agreement is indeed observed.

Let us examine these data in more details. First, since the $\beta-\alpha$ amplitude is dominated by the product $R_{\alpha,1}R_{\beta,1}$ (see equation (A.5)) its temperature dependence displays a slightly negative curvature. Analyzed through the LK formula, the data would yield an apparent effective mass $m^{\rm app}_{\beta-\alpha}$ close to that of $\beta+\alpha$, actually about $0.8(m_\beta+m_\alpha)$. This result is in agreement with both experimental data relevant to κ-$ET_2Cu(NCS)_2$ for which $m^{\rm app}_{\beta-\alpha}\simeq 0.85(m_\beta+m_\alpha)$ [7], and in line with numerical simulations [16].

As already observed [5, 7, 39], 2α is not accounted for by the LK formula as well. Indeed, according to equation (A.2), the second-order term which is of the same order of magnitude as the LK damping factor $R_{\alpha,2}$ is dominated by $R^2_{\alpha,1}$ accounting for a non-LK behaviour.

Oppositely, the amplitude of the $2\beta-\alpha$ component is very close to the prediction of the LK model since the second-order term, dominated by the product $R_{\alpha,1}R_{\beta,2}$ is very small compared to the LK term which is proportional to $R_{2\beta-\alpha,1}$.

Finally, the Fourier component $\beta+\alpha$ is considered in figure 6. While below about 2.6 K, the amplitude decreases as the temperature decreases, it increases in the range 2.6 K ∼ 3.5 K, in strong discrepancy with the LK formula. This behaviour is quantitatively well accounted for by equation (A.7)

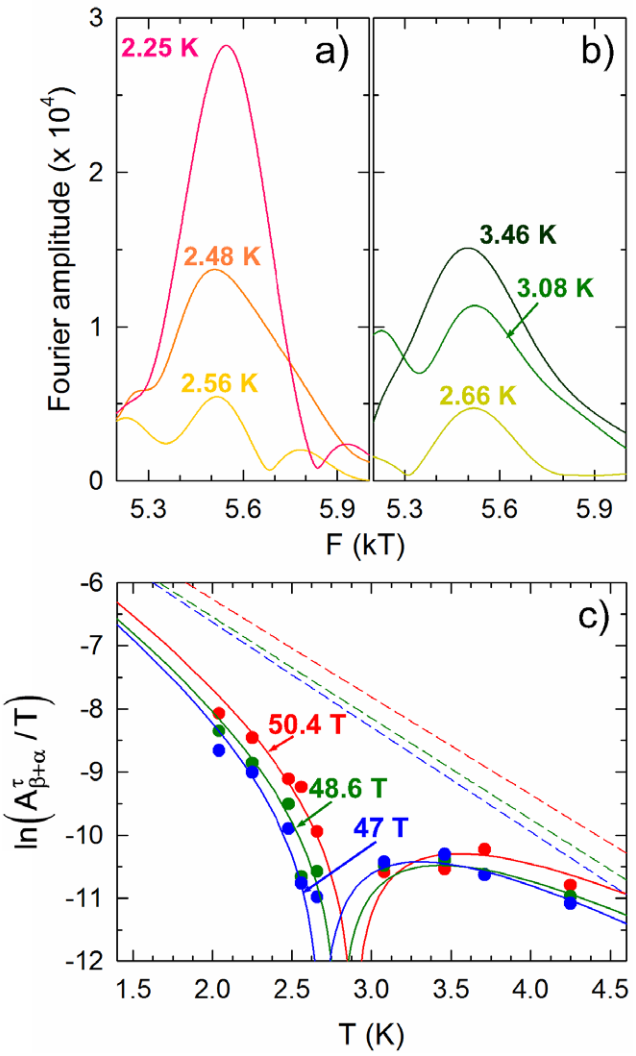

Figure 6. Fourier analysis in the frequency range around $F_{\beta+\alpha}$, at the mean magnetic field value $\bar{B}=47$ T. In the temperature range (a) 2.25–2.56 K and (b) 2.66–3.48 K, the Fourier amplitude decreases and increases, respectively, as the temperature increases. (c) Mass plot for different values of the magnetic field. Solid lines are calculated with equation (A.7). They are obtained with the same set of parameters as in figures 2, 3 and 5. Dotted lines are the contributions of the first-order term, corresponding to the Lifshitz–Kosevich formula.

which evidences a dip in the temperature dependence of the amplitude. Indeed, the second-order term of equation (A.7) is dominated by the product $R_{\alpha,1}R_{\beta,1}$ which contributes to the amplitude with an opposite sign to the first-order Lifshitz–Kosevich term proportional to $R_{\alpha+\beta,1}$. These two factors cancel each other at a given field and temperature value (e.g. 2.9 K at 50 T in the present case), depending on the spin damping factors value, hence on the respective values of the products $g^*_\alpha m_\alpha$ and $g^*_\beta m_\beta$. It can be remarked that this feature is not observed in the Co-compound [17]. Indeed, owing to slightly different effective masses and effective Landé factors, the dip in the $\beta+\alpha$ amplitude would be observed around 9 K, i.e. beyond the temperature range in which oscillations can be observed [19].

4. Summary and conclusion

Band structure calculations relevant to the quasi-two dimensional metal θ-$(ET)_4ZnBr_4(C_6H_4Cl_2)$ indicate that this compound illustrates the linear chain of coupled orbits model proposed by Pippard [1, 2] (see figure 1) as it is the case for many organic conductors based on the ET molecule. In line with this statement, quantum oscillations spectra evidence many Fourier components, the frequency of which are linear combinations of the frequencies relevant to the closed α and the magnetic breakdown β orbits. The field and temperature dependence of the de Haas–van Alphen amplitude of these components is quantitatively accounted for by the analytic calculations reported in the Appendix. Beyond the Lifshitz–Kosevich formula, they include second-order terms arising from the chemical potential oscillations. These second-order terms have negligible contributions to the amplitude of the basic α and β components allowing the determination of the various physical parameters entering the data (effective masses, magnetic breakdown fields, etc). They have also a minor contribution on the magnetic breakdown orbit $2\beta-\alpha$. Oppositely, they have significant contribution to 2α and $\beta+\alpha$. Although this latter component physically corresponds to a magnetic breakdown orbit, its temperature dependence evidences a strong dip due to the cancelation of the first and second-order terms. Finally, the 'forbidden frequency' $\beta-\alpha$ and its harmonic $2\beta-2\alpha$, which are due to the oscillation of the chemical potential, are accordingly accounted for by second-order terms, only.

Acknowledgments

Part of the x-ray diffraction experiments have been performed at the Laboratoire de Chimie de coordination of Toulouse with the help of L Vendier. The support of the European Magnetic Field Laboratory (EMFL) is acknowledged. Work in Bellaterra was supported by MINECO through grant FIS2012-37549-C05-05 and Generalitat de Catalunya (2014SGR301). Work in Chernogolovka was supported by grant of Presidium RAS 1.1.1.9.

Appendix A. Analytical expressions of Fourier amplitudes

In this appendix, are recalled the analytical equations for de Haas–van Alphen amplitudes $A_{p\eta}$ with frequencies pF_η given in [17–19]. They are relevant to two-dimensional FS illustrating the Pippard model in which the component η is a linear combination of the α and β orbits and p is the harmonic order (see insert of figure 1).

$$A_\alpha = -\frac{F_\alpha}{\pi m_\alpha}R_{\alpha,1} - \frac{F_\alpha}{\pi m_\beta}\left[\frac{1}{2}R_{\alpha,1}R_{\alpha,2} + \frac{1}{6}R_{\alpha,2}R_{\alpha,3} + 2R_{\beta,1}R_{\alpha+\beta,1} + \frac{1}{2}R_{\beta,2}R_{2\beta-\alpha,1}\right] \tag{A.1}$$

$$A_{2\alpha} = -\frac{F_\alpha}{2\pi m_\alpha}R_{\alpha,2} + \frac{F_\alpha}{\pi m_\beta}\left[R_{\alpha,1}^2 - \frac{2}{3}R_{\alpha,1}R_{\alpha,3} - R_{\alpha,2}R_{\alpha+\beta,2}\right] \tag{A.2}$$

$$A_\beta = -\frac{F_\beta}{\pi m_\beta}R_{\beta,1} - \frac{F_\beta}{\pi m_\beta}\left[\frac{1}{2}R_{\beta,1}R_{\beta,2} + \frac{1}{6}R_{\beta,2}R_{\beta,3} + 2R_{\alpha,1}R_{\alpha+\beta,1} + 2R_{\beta,1}R_{2\beta,1}\right] \tag{A.3}$$

$$A_{2\beta} = -\frac{F_\beta}{2\pi m_\beta}[R_{\beta,2} + 2R_{2\beta,1}] + \frac{F_\beta}{\pi m_\beta}\left[R_{\beta,1}^2 - \frac{2}{3}R_{\beta,1}R_{\beta,3} - \frac{1}{4}R_{\beta,2}R_{\beta,4} - R_{\alpha,2}R_{\alpha+\beta,2} + 2R_{\alpha,1}R_{2\beta-\alpha,1} - R_{\beta,2}R_{2\beta,2} - R_{\beta,4}R_{2\beta,1}\right] \tag{A.4}$$

$$A_{\beta-\alpha} = -\frac{F_{\beta-\alpha}}{\pi m_\beta}[R_{\alpha,1}R_{\beta,1} + R_{\alpha,2}R_{\alpha+\beta,1} + R_{\beta,2}R_{\alpha+\beta,1} + R_{\beta,1}R_{2\beta-\alpha,1}] \tag{A.5}$$

$$A_{2(\beta-\alpha)} = -\frac{F_{2\beta-2\alpha}}{\pi m_\beta}\left[2R_{\alpha,2}R_{2\beta,1} + 2R_{2\beta-\alpha,2}R_{2\beta,1} + 2R_{\alpha,1}R_{2\beta-\alpha,1} + \frac{1}{2}R_{\alpha,4}R_{\alpha+\beta,2} + \frac{1}{2}R_{\alpha,2}R_{\beta,2} + \frac{1}{2}R_{\beta,2}R_{2\beta-\alpha,2}\right] \tag{A.6}$$

$$A_{\beta+\alpha} = -\frac{2F_{\beta+\alpha}}{\pi m_{\beta+\alpha}}R_{\beta+\alpha,1} + \frac{F_{\beta+\alpha}}{\pi m_\beta}\left[R_{\alpha,1}R_{\beta,1} - 2R_{\alpha+\beta,2}R_{\alpha+\beta,1} - \frac{1}{3}R_{\beta,3}R_{2\beta-\alpha,1}\right] \tag{A.7}$$

$$A_{2\beta-\alpha} = -\frac{F_{2\beta-\alpha}}{\pi m_{2\beta-\alpha}}R_{2\beta-\alpha,1} - \frac{F_{2\beta-\alpha}}{\pi m_\beta}\left[\frac{1}{2}R_{\alpha,1}R_{\beta,2} + \frac{1}{3}R_{\alpha,3}R_{\alpha+\beta,2}\right] \tag{A.8}$$

Damping factors are given by the LK and coupled orbits network models [2] as $R_{\eta,p}(B,T) = R^{\mathrm{T}}_{\eta,p}(B,T)R^{\mathrm{D}}_{\eta,p}(B)R^{\mathrm{MB}}_{\eta,p}(B)R^{\mathrm{s}}_{\eta,p}$ [2, 3] where the temperature, Dingle, MB and spin damping factors are expressed as $R^{T}_{\eta,p} = pX_\eta \sinh^{-1}(pX_\eta)$, $R^{\mathrm{D}}_{\eta,p} = \exp(-pu_0m_\eta T_{\mathrm{D}}(B\cos\theta)^{-1})$, $R^{\mathrm{MB}}_{\eta,p} = (\mathrm{i}p_0)^{n^t_\eta}(q_0)^{n^r_\eta}$, $R^{\mathrm{s}}_{\eta,p} = \cos(\pi g^*_\eta m_\eta/2\cos\theta)$, respectively. The field-and temperature-dependent variable (X_η) and the constant (u_0) are expressed as $X_\eta = u_0m_\eta T/(B\cos\theta)$ and $u_0 = 2\pi^2k_{\mathrm{B}}m_e(e\hbar)^{-1} = 14.694\ \mathrm{T\ K^{-1}}$. The tunneling (p_0) and reflection (q_0) probabilities are given by $p_0 = \mathrm{e}^{-B_0/2B\cos\theta}$ and $p_0^2 + q_0^2 = 1$. T_{D} is the Dingle temperature defined by $T_{\mathrm{D}} = \hbar(2\pi k_{\mathrm{B}}\tau)^{-1}$, where τ^{-1} is the scattering rate, B_0 is the MB field, m_η and g^*_η are the effective mass and effective Landé factor, respectively. It can be noticed that the terms of first order in damping factors correspond to the LK model.

References

[1] Pippard A B 1962 *Proc. R. Soc.* A **270** 1
[2] Shoenberg D 1984 *Magnetic Oscillations in Metals* (Cambridge: Cambridge University Press)
[3] Falicov L M and Stachowiak H 1966 *Phys. Rev.* **147** 505
[4] Kartsovnik M 2004 *Chem. Rev.* **104** 5737
[5] Uji S and Brooks J S 2008 *The Physics of Organic Superconductors and Conductors* (*Springer Series Material Science* vol 110) (Berlin: Springer) p 89
[6] Harrison N, Caulfield J, Singleton J, Reinders P H P, Herlach F, Hayes W, Kurmoo M and Day P 1996 *J. Phys.: Condens. Matter.* **8** 5415
[7] Uji S, Chaparala M, Hill S, Sandhu P S, Qualls J, Seger L and Brooks J S 1997 *Synth. Met.* **85** 1573
[8] Steep E, Nguyen L H, Biberacher W, Müller H, Jansen A G M and Wyder P 1999 *Physica* B **259–61** 1079
[9] Caulfield J, Lubczynski W, Pratt F L, Singleton J, Ko D Y K, Hayes W, Kurmoo M and Day P 1994 *J. Phys.:Condens. Matter.* **6** 2911
[10] Alexandrov A S and Bratkovsky A M 1996 *Phys. Rev. Lett.* **76** 1308
[11] Fortin J Y and Ziman T 1998 *Phys. Rev. Lett.* **80** 3117
[12] Alexandrov A S and Bratkovsky A M 2001 *Phys. Rev.* B **63** 033105
[13] Champel T 2002 *Phys. Rev.* B **65** 153403
[14] Kishigi K and Hasegawa Y 2002 *Phys. Rev.* B **65** 205405
[15] Gvozdikov V M, Pershin Y V, Steep E, Jansen A G M and Wyder P 2002 *Phys. Rev.* B **65** 165102
[16] Fortin J Y, Perez E and Audouard A 2005 *Phys. Rev.* B **71** 15501
[17] Audouard A *et al* 2012 *Europhys. Lett.* **97** 57003
[18] Audouard A, Fortin J-Y, Vignolles D, Lyubovskii R B, Zhilyaeva E I, Lyubovskaya R N and Canadell E 2013 *Synth. Met.* **171** 51
[19] Audouard A and Fortin J-Y 2014 *Low Temp. Phys.* **40** 344–51
Audouard A and Fortin J-Y 2014 *Fiz. Nizk. Temp.* **40** 444–53
[20] Stark R W and Friedberg C B 1971 *Phys. Rev. Lett.* **26** 556
[21] Kartsovnik M V, Logvenov G Yu, Ishiguro T, Biberacher W, Anzai H and Kushch N D 1996 *Phys. Rev. Lett.* **77** 2530
[22] Lyubovskaya R, Zhilyaeva E, Shilov G, Audouard A, Vignolles D, Canadell E, Pesotskii S and Lyubovskii R 2014 *Eur. J. Inorg. Chem.* **2014** 3820
[23] Shilov G V, Zhilyaeva E I, Flakina A M, Torunova S A, Lyubovskii R B, Aldoshin S M and Lyubovskaya R N 2011 *Cryst. Eng. Commun.* **13** 1467
[24] Whangbo M-H and Hoffmann R 1978 *J. Am. Chem. Soc.* **100** 6093
[25] Pénicaud A, Boubekeur K, Batail P, Canadell E, Auban-Senzier P and Jérome D 1993 *J. Am. Chem. Soc.* **115** 4101
[26] Audouard A, Duc F, Vignolles D, Lyubovskii R B, Vendier L, Shilov G V, Zhilyaeva E I, Lyubovskaya R N and Canadell E 2011 *Phys. Rev.* B **84** 045101
[27] Drigo L, Durantel F, Audouard A and Ballon G 2010 *Eur. Phys. J.: Appl. Phys.* **52** 10401
[28] Shibaeva R P and Yagubskii E B 2004 *Chem. Rev.* **104** 5347
[29] Kobayashi A, Kato R, Kobayashi H, Moriyama S, Nishio Y, Kajita K and Sasaki W 1986 *Chem. Lett.* **15** 2017
[30] Coffey T, Bayindir Z, DeCarolis J F, Bennett M, Esper G and Agosta C C 2000 *Rev. Sci. Instrum.* **71** 4600
[31] Ohmichi E, Komatsu E and Osada T 2004 *Rev. Sci. Instrum.* **75** 2094
[32] Laukhin V N *et al* 1995 *Physica* B **211** 282
[33] Sandhu P S, Athas G J, Brooks J S, Haanappel E G, Goettee J D, Rickel D W, Tokumoto M, Kinoshita N, Kinoshita T and Tanaka Y 1996 *Surf. Sci.* **361–2** 913
[34] Harrison N, Bogaerts R, Reinders P H P, Singleton J, Blundell S S and Herlach F 1996 *Phys. Rev.* B **54** 9977
[35] Grigoriev P D 2003 *Phys. Rev.* B **67** 144401
[36] Thomas I O, Kabanov V V and Alexandrov A S 2008 *Phys. Rev.* B **77** 075434
[37] Berkutov I B, Andrievski V V, Komnik Yu F, Mironov O A, Mironov M and Leadley D R 2009 *Low Temp. Phys.* **35** 141
[38] Endo A, Hatano N, Nakamura H and Shirasaki R 2009 *J. Phys.: Condens. Matter* **21** 345803
[39] Wosnitza J, Gvozdikov V M, Hagel J, Ignatchik O, Bergk B, Meeson P J, Schlueter J A, Davis H, Winter R W and Gard G L 2008 *New J. Phys.* **10** 083032